

FORMING DISK GALAXIES IN WET MAJOR MERGERS. I. THREE FIDUCIAL EXAMPLES

E. ATHANASSOULA, S. A. RODIONOV, N. PESCHKEN, J. C. LAMBERT

Laboratoire d’Astrophysique de Marseille (LAM), UMR7326, CNRS/Aix Marseille Université, Technopôle de Marseille-Etoile,
38 rue Frédéric Joliot Curie, 13388 Marseille Cédex 13, France

(Received; Revised; Accepted)
Draft version October 9, 2018

ABSTRACT

Using three fiducial Nbody+SPH simulations, we follow the merging of two disk galaxies with a hot gaseous halo component each, and examine whether the merger remnant can be a spiral galaxy. The stellar progenitor disks are destroyed by violent relaxation during the merging and most of their stars form a classical bulge, while the remaining form a thick disk and its bar. A new stellar disk forms subsequently and gradually in the remnant from the gas accreted mainly from the halo. It is vertically thin and well extended in its equatorial plane. A bar starts forming before the disk is fully in place, contrary to what is assumed in idealised simulations of isolated bar-forming galaxies. It has morphological features such as ansae and boxy/peanut bulges. Stars of different ages populate different parts of the box/peanut. A disk pseudobulge forms also, so that by the end of the simulation, all three types of bulges coexist. The oldest stars are found in the classical bulge, followed by those of the thick disk, then by those in the thin disk. The youngest stars are in the spiral arms and the disk pseudobulge. The disk surface density profiles are of type II (exponential with downbending), and the circular velocity curves are flat and show that the disks are submaximum in these examples: two clearly so and one near-borderline between maximum and submaximum. On average, only roughly between 10 and 20% of the stellar mass is in the classical bulge of the final models, i.e. much less than in previous simulations.

Subject headings: galaxies: structure — galaxies: kinematics and dynamics — galaxies: spiral

1. INTRODUCTION

What results from a merger of two disk galaxies of comparable mass? Toomre & Toomre (1972) were the first to propose that such a merger will form an elliptical. After some strong initial rebuttals, this was generally accepted (see e.g. Barnes 1998 and Schweizer 1998 for reviews), only to be questioned again in the last decade. Indeed, several observations at intermediate redshifts, suggest that the result of a merging of two gas-rich disk galaxies of comparable luminosity is actually not an elliptical, but a disk galaxy (e.g. Hammer et al. 2005, 2009a,b). Roughly concurrently, pioneering and seminal numerical simulations showed that the remnants of mergers of gas-rich disk galaxies do have a disk component (e.g. Barnes 2002, Springel & Hernquist 2005, Cox et al. 2006, Robertson et al. 2006, Lotz et al. 2010b, Governato et al. 2009, Hopkins et al. 2009, 2013, Wang et al. 2012, Borlaff et al. 2014, Querejeta et al. 2015). However, the relative mass and/or extent of these disks are in general considerably smaller than those of present day spiral galaxy disks. This formation mechanism could thus perhaps be appropriate for lenticulars, but not for spirals. Furthermore, although bars are present in about two thirds of disk galaxies in the local universe (Eskridge et al. 2000; Knapen et al. 2000; Menéndez-Delmestre et al. 2007; Buta et al. 2015, etc.) and are believed to be a major driver of secular evolution (see e.g. Athanassoula 2013; Kormendy 2013, for reviews of the theoretical and observational parts, respectively), these works provide little or no information on whether and when major merger remnants can have bars and on whether their bar properties and parameters are realistic.

It is thus necessary to return to this still open question

and to test whether the remnants of major mergers could be spiral galaxies with the appropriate morphology, mass distribution, kinematics and substructures. In this paper, the first of a series, we present first results for three fiducial wet major merger simulations and their remnants. We first present the improvements we introduce in the modeling of the protogalaxies and in the simulation resolution and give information on the code we used and our initial conditions (Sect. 2). Sect. 3 presents and discusses our results. We show that the disk of the remnant can extend over several scale-lengths, while the B/T ratio (classical-bulge-to-total stellar mass ratio) can reach sufficiently low values to be representative of spirals. We also discuss morphologies, including those of spirals and bars, show rotation curves and projected density radial profiles, and discuss when and how the various components are produced. We compare the morphology and kinematics of stellar populations with different ages (Sect. 3.6) and also present a simple scenario for the formation of disk galaxies (Sect. 4), before summarizing and concluding (Sect. 5). The nomenclature used in this paper is summarized in the Appendix. For brevity, we will hereafter often refer to our simulated galaxies simply as “galaxies”, and to stellar particles in the simulation as “stars”.

2. SIMULATIONS

2.1. General context

Compared to previous simulations on this specific subject, ours present one numerical and one conceptual advantage.

As a numerical advantage, we have a much better resolution than previous simulations tackling the specific question that we have set out to address in this project, namely whether major mergers of gas rich disk galaxies can form spirals, or not. Indeed, to answer this question necessitates a survey of simulations, as e.g. in Hopkins et al. (2009), so that the use of high resolution becomes computationally much more expen-

sive than for problems necessitating only few simulations. For this reason previous attempts restricted themselves to considerably less than or of the order of half a million particles in total.¹ We increased this number by more than an order of magnitude, adopting for each gas, or stellar particle a mass of $m_g = 5 \times 10^4 M_\odot$ and a softening of 25 pc. The dark matter (DM) particles have a mass of $m_{\text{DM}} = 2 \times 10^5 M_\odot$ and a softening of 50 pc. We thus have in our simulations 2 and 3.5 million particles for the baryons and DM, respectively.

The conceptual improvement concerns the initial conditions of the simulations. In previous works, the progenitors resembled local disk galaxies, except for a higher content of cold gas in the disk. They consisted of a DM halo, a disk and sometimes a classical bulge with properties compatible to those of local galaxies. It is, however, well established that disk galaxies, except for the cold gas in their disk, have also hot gas in their halos (e.g. Miller & Bregman 2015). To include this, we start off our simulations with spherical protogalaxies consisting of DM and hot gas. Before the merging, a disk forms in each of the progenitors, so that we witness the merging of two disc proto-galaxies. The two gaseous halos merge into a single one enveloping the remnant and thus halo gas accretes onto the remnant disk all through the simulation (Sect. 3.2). Such gaseous halos exist also in mergings occurring in cosmological simulations (e.g. Governato et al. 2009), or in a couple of major merger studies (Moster et al. 2011; Kannan et al. 2015), whose remnants have a B/T ratio between 0.7 and 1., thus linking them to ellipticals with a small disk. Thus, to our knowledge, our study is the first one to include a hot gaseous component in dynamical simulations of major mergers whose remnants model realistic spiral galaxies.

2.2. Code

A full discussion of the code used in these simulations and of their initial conditions is the subject of the next paper in this series (Rodionov et al., in prep., Paper II). In this and the next two subsections we only summarise the main information necessary here.

We use a version of GADGET3 including gas and its physics (Springel & Hernquist 2002; Springel 2005). DM and stars are modeled by N-body particles, and gravity is calculated with a tree code. The code uses an entropy conserving density driven formulation of SPH with adaptive smoothing lengths (Springel & Hernquist 2002) and subgrid physics (Springel & Hernquist 2003).

Our feedback, star formation and cooling follow subgrid physics included in simple recipes given by Springel & Hernquist (2003) and were already used in a number of previous works cited in Sect. 1. It is beyond the scope of this paper to test other subgrid physics. Nevertheless, let us mention briefly that Cox et al. (2006) showed that the mass profiles of the major merger remnants are robust to substantial changes in subgrid physics parametrizations. Similarly, Hopkins et al. (2009) find that the efficiency with which gas avoids consumption during the merger and can reform a disk does not depend on the subgrid parametrization, unless the feedback is very weak. Most important, Hopkins et al. (2013) introduced

detailed, explicit models for stellar feedback in their very high resolution major merger simulations and found that in all cases the mass profile results of explicit feedback models are nearly identical to those obtained with the subgrid physics we use here, except for some second order differences.

2.3. Central, AGN-like feedback

The code described above has already been used a large number of times to test the relevance of major mergers regarding the formation of disk galaxies, as e.g. in Hopkins et al. (2009, and references therein), albeit with initial conditions that do not include gaseous halos. We also used it in a number of our simulations, which always include gaseous halos. In those cases, we obtained merger remnants which are disk galaxies with thin and extended disks and realistic spiral arms, but with one serious drawback which is that the centermost part of the galaxy had a considerable central concentration, leading to an unrealistically high inner maximum of the circular velocity curve (Paper II). Furthermore, this high central mass concentration has the disadvantage of prohibiting bar formation, or at least delaying it beyond the 10 Gyr covered by our simulations. This is in disagreement with observations, since about 2/3 of local disk galaxies are barred (see references in Sect. 1).

Such excessive concentrations were also obtained in cosmological simulations of disk galaxy formation and were lately addressed by introducing additional feedback in the central regions, mainly in the form of AGN feedback. Very schematically, in this picture gas will flow inwards to the central black hole (BH). Feedback is then calculated as a given fraction of the luminosity which is radiated by the BH. This energy is distributed to the gas in the central region in the form of thermal energy, thus preventing excessive star formation.

In most studies, the inflow on to the BH is modeled using the Bondi accretion formalism (Hoyle & Lyttleton 1939; Bondi & Hoyle 1944; Bondi 1952), sometimes limiting it by the Eddington accretion rate to prevent excessive accretion. This inflow formalism has two free parameters, the accretion efficiency and the radiative efficiency (Springel et al. 2005). However, the physics of driving BH-generated outflows is still not well understood (e.g. Silk & Mamon 2012), and also necessitates resolutions much higher than what we have here. It has, furthermore, been criticized by Hopkins & Quataert (2012), who calculated the accretion directly from subparsec ‘resimulations’ of the central region of galaxy-scale simulations.

Our approach is based on the same physics, but since all we want is to solve the excessive mass concentration problem and not to model the BH accurately, we adopted a very straightforward, empirical and parametric method. As gas flows inwards, it will increase the density in the central regions. As in previous descriptions, we introduce two parameters, a density threshold ρ_{AGN} and a temperature T_{AGN} . More specifically, at every time step we give internal energy to gas particles whose local density is larger than the threshold ρ_{AGN} , by increasing their temperature to T_{AGN} . This density threshold is chosen so as to ensure that the chosen particles are located in the centermost region. Furthermore, to ensure that the amount of energy that we thus inject is not excessive, we test at every step that the total energy distributed is below that of the Eddington rate (see e.g. Springel et al. 2005). We do this in a probabilistic manner, by setting the probability of a particle receiving internal energy equal to 1 if the energy to be distributed is less than the Eddington limit, or, if it is higher than

¹ Amongst the simulations with a resolution yet higher than ours we note two simulations of Milky Way sized galaxies with a resolution of four pc, i.e. roughly six times better than ours (Hopkins et al. 2013). Such a resolution, however, would be impossible for our project, since a few hundred simulations are necessary for an even cursory examination of the parameter space and in order for the three simulations discussed here to be fiducial they need to have the same resolution as the rest.

that limit, setting the probability as the ratio of the Eddington limit to the energy we were initially to distribute. A fuller description will be given in Paper II, where we describe all our computational and technical aspects in detail. Although very simple, this description includes the essentials sufficient for our purposes, namely it injects energy in the central regions to prevent excessive star formation. Compared to cases with no AGN feedback, it leads to mass distributions which are less concentrated in the centermost parts, more realistic circular velocity curves and allows bars to grow.

In our scheme there is no single particle representing the BH, as any spurious off-centering of such a particle, or its imperfect correction by analytical drag forces, could introduce errors because the BH mass is so much higher than that of the other particles in the simulation. Nevertheless, it is useful to keep track of the evolution of the BH mass (M_{BH}) with time. We do this by measuring the energy released by our AGN-like feedback as a function of time and then following the simple formalism described in Springel et al. (2005, p. 783).

The following three questions need to be considered here:

1. *Does the thus described feedback model lead to unphysical results?* Several arguments argue against this:

- The shape of the circular velocity curve, from unrealistic as in simulations without this central feedback, becomes very realistic, well compatible with observed rotation curves.
- The mass of the BH at the end of the simulation, calculated using the energy of the feedback, is 1., 1.4 and $3.3 \times 10^7 M_{\odot}$ for our three fiducial simulations. These are reasonable values for disk galaxies. Moreover, we calculated the velocity dispersion of the central parts, σ , directly from our simulation and found that this (M_{BH}, σ) pair falls near the $M_{\text{BH}} - \sigma$ relation (Ferrarese & Merritt 2000; Gebhardt et al. 2000), within the observational spread.
- Qualitatively, the evolution of M_{BH} during the merging is similar to that obtained with other AGN feedback prescriptions, namely increases much more sharply during the merging than after it (e.g. Thacker et al. 2014).
- Last, but not least, we ensure that at all times the amount of injected energy does not exceed the Eddington limit as described above.

2. *How is this energy distributed?* We followed during the simulations the locations of the gas particles to which the energy is deposited. We found that these particles cover a region around the dynamical center of the halo, i.e. around the position of the halo particle with the highest local density. The area they cover may vary from one run to another, but it is always much larger during the merging times. At such times, their characteristic size is of the order of half to one kpc, but becomes considerably smaller after the merging, when it is of the order of say 100 pc. This increase of the characteristic size during merging reflects the corresponding much larger feedback, while the extent during the merging time can be compared to the circumnuclear region which is very active during a merging (see e.g. Scoville et al. 1991 for the merging system Arp 220).

3. *Does this feedback affect the simulation results?* Indeed it does, as expected and required. Namely it changes the shape of the circular velocity curve, making it compatible with observations and, as a corollary, it allows the formation of bars, which we know are present in the majority of nearby galaxies (see references in Sect. 1). Moreover, changes in the values of the two adopted parameter (ρ_{AGN} and T_{AGN}) should, and do, affect the simulation results. This is expected since they change the shape of the circular velocity curve and thus the bar properties, which, in turn, influences the dynamics and structure at least in the inner parts of the disk. These changes are most important in the central region hosting the bar, but much smaller at larger radii (Paper II).

To summarise, our simple parametric description of the central feedback has the desired effect without being unphysical. We thus adopt it for our simulations.

2.4. Further information on the code

Making a full comparison of the results of our simulations with those obtained with other codes, but with the same initial conditions and the same gas physics and subgrid physics, is beyond the scope of this paper. We, nevertheless, reran one of our fiducial simulation (referred to in the following as mdf732, see Sect. 2.6) using the GIZMO code (Hopkins 2013, 2014, 2015), after implementing to it the subgrid physics we use here. This code is a derivative code of GADGET, using the same MPI parallelization, domain decomposition, gravity solvers, etc. However, in contrast to that of GADGET, the SPH version of GIZMO is density independent, and it also includes a more sophisticated treatment of the artificial viscosity term (Cullen & Dehnen 2010), as described in Hopkins (2013, Sect. 3.1). It can thus handle better the phase boundaries, e.g. between the hot gas in the halo and the much cooler gas in the disk, or the description of cold dense clumps of gas in the otherwise hot halo.

The main difference we found between the results of these two codes is in the hot gaseous halo. This has small gaseous clumps in the simulation run with GADGET3, which are either absent, or much less prominent in the GIZMO run (see also Torrey et al. 2012 and Hayward et al. 2014). On the other hand, we find very good agreement when we compare the properties of the remnants, e.g. their gaseous or stellar projected density radial profile, their cumulative stellar mass, or the mean tangential velocity of the stars or gas and the stellar radial and vertical velocity dispersion profiles.

The good agreement between the properties of these two simulations argues that the clumps present in the halo of the GADGET simulation do not influence much the behaviour of the stellar component. Even the stellar vertical velocity dispersion or the thickness of the stellar disk are in good agreement, which shows that these clumps are not sufficiently massive and/or numerous to heat up noticeably the stellar disk.

2.5. Initial density profiles of the protogalaxies

We used idealised initial conditions with two identical protogalaxies composed of spherical DM and gaseous halos, of masses M_{DM} and M_{gas} , respectively, with $M_{\text{total}}/M_{\text{gas}} = 8$. The initial density of the DM and the gaseous halo is

$$\rho(r) = C \operatorname{sech}(r/r_t) x^{-\gamma_i} (x^\eta + 1)^{-(\gamma_o - \gamma_i)/\eta}, \quad (1)$$

where r is the spherical radius, $x = r/a$ and a and r_t are the scalelength and tapering radius of the halo, respectively.

The constants γ_i, γ_o and η characterize the shape of the radial density profile. The DM halo has $\gamma_i = 1, \gamma_o = 3$ and $\eta = 1$, while the gaseous one has $\gamma_i = 0, \gamma_o = 2$ and $\eta = 2$ (Beta model for $\beta = 2/3$, e.g. Miller & Bregman 2015 and references therein). For both we have $r_t=100$ kpc and $a=14$ kpc. The halo component was built following McMillan & Dehnen (2007), i.e. with a Cuddeford (1991) distribution function. We also add a small amount of spin to the halo. Let f be the fraction of particles with a positive sense of rotation. In cases with no net rotation $f=0.5$, while if all particles rotate in the positive (negative) sense $f=1$ (-1). The internal energy of the gas was set by requiring hydrostatic equilibrium (Paper II).

Stars do not exist in the initial conditions, but form during the evolution, so that, at the time of the merging, a stellar and a gaseous disk are present in the progenitor galaxies. Thus their density and velocity profiles are set by our initial setup for the hot halo gas distribution and its subsequent evolution, and not directly by the modeller seeking to match e.g. what is measured in nearby galaxies.

2.6. Three fiducial examples

In this paper we discuss three simulations (mdf732, mdf778 and mdf780). All three are 1:1 mergers of two identical protogalaxies. We start by adopting the simple case of coplanar mergers, while other orientations will be considered in forthcoming studies. We just mention briefly here that preliminary results show, as expected, that the orientations of the spin axes with respect to the orbital plane influence considerably the properties of the remnant, and that this may account for the spread observed in disk sizes, B/T ratios and gas fractions of nearby galaxies.

The orbits of the centers of density of the two protogalaxies, i.e. the orbits of the location where their DM density is highest, are given in Fig. 1a. Simulations mdf732 and mdf780 have $f=0.6$ and mdf778 has 0.55. The adopted AGN parameters are $\rho_{AGN}=1 M_{\odot}/pc^3$ for all three cases, and $T_{AGN}=10^7$ K for mdf732 and mdf778, and 2.5×10^7 K for mdf780. We continued all simulations up to 10 Gyr.

3. RESULTS AND DISCUSSION

3.1. Early evolution of individual isolated galaxies

In previous works (see papers cited in Sect. 1), the initial conditions consisted of two fully developed disk galaxies set on a given trajectory. Each consisted of a spherical halo, an exponential stellar disk and, in some cases, a classical bulge and/or a gaseous disk. Their properties were chosen so as to represent nearby galaxies; except for the fraction of gas in the disk, which was a free parameter varied at will. Thus gas fractions in the complete range between 0 and 1 were tried, even if this was not necessarily compatible with e.g. the adopted disk scale length (which was most times appropriate for low-redshift Milky-Way-like disk galaxies, i.e. 3 to 5 kpc), or with their B/T mass fraction. Although not ideal, these initial conditions allowed previous works to reach interesting conclusions, for example on the crucial role of the initial gas fraction on the nature of the merger remnant. This is presumably due to the fact that violent relaxation occurring during the merging wipes out all small details of the initial stellar structures.

We chose to start out with very different initial conditions for the progenitors (Sect. 2). However, before using these initial conditions in our major merger simulations we made sure that, when evolved in isolation, their $t=10$ Gyr snapshots

gave reasonable approximations of local disk galaxies, and that during their early stages of evolution (up to say 2 Gyrs) they were compatible with the main properties of disk galaxies at such times. The latter entails that the disk should be considerably smaller and more perturbed than the disks in local isolated galaxies and that the fraction of gas in their disk should be higher (Bouwens et al. 2004; Ferguson et al. 2004; Elmegreen et al. 2005; Dahlen et al. 2007; Erb et al. 2006; Leroy et al. 2008; Daddi et al. 2010; Tacconi et al. 2010; Conselice et al. 2012; Rodrigues et al. 2012; Genzel et al. 2015, etc). More information on all this will be given elsewhere (Peschken et al., in prep.), but we summarise below some relevant information.

In our simulations, the protogalaxies at $t=0$ consist only of spherical distributions of DM and gas (Sect. 2.5). From the onset of the simulation, however, the gas in the halo cools radiatively and, getting out of equilibrium, falls inwards. Its density increases locally and the first stars form. Thus, the progenitors gradually acquire a disk. This, as expected, is much more perturbed and lumpy than the more settled exponential disks to which it evolves at later times. Fig. 2a shows the radial surface density profile at five times during the evolution (0.5, 1, 2, 5 and 10 Gyr). It is clear that the disk grows inside-out, relatively fast at early times and less so later on. The profiles are initially exponential-like, but it is not trivial to measure adequately their scale-length, so, instead, we measure the cylindrical radius R_{70} , containing 70% of the stellar mass. It is clear that this quantity increases considerably with time, as expected, particularly at early evolution stages (Fig. 2b).

Fig. 2c shows the fraction of gas in the disk component measured within $|\Delta z| < 0.5$ kpc. We see that at the relevant times, i.e. the times corresponding to before the merging, the gas fractions are in the ballpark of 60 to 30%, i.e. considerably larger than the corresponding gas fractions in nearby disk galaxies, in good agreement with observations of both local and intermediate redshift galaxies.

We do not claim that this is a perfect model of galaxies at intermediate redshifts, but it is still a considerable improvement over those used in previous studies. This improvement is a corollary of the existence of a hot gaseous halo in our initial conditions, as this entails a slow formation and evolution of the disk which becomes gradually more massive and more extended, while the gas fraction in the disk decreases monotonically with time.

3.2. General evolution of a major merger

The stellar disks of the progenitor galaxies are destroyed by the merging and their stars concentrate in the central regions of the remnant. As we will see in the following sections most of them form a classical bulge, while the remaining, albeit much smaller number of stars, contribute to a thick disk and its bar. The gaseous disks of the progenitors are also destroyed, and the gas which they included also concentrates in the innermost regions of the remnant, so that the stars that form from it contribute to the classical or disky pseudobulge.

After the end of the merging, gas continues to fall in mainly from the halo, but also, although in much smaller quantities, from the gaseous tails formed during the interaction. Thus a new disk is gradually formed, which very early on shows well-defined spiral arms. This gas accretion continues all through the simulation.

3.3. Morphology of merger remnants

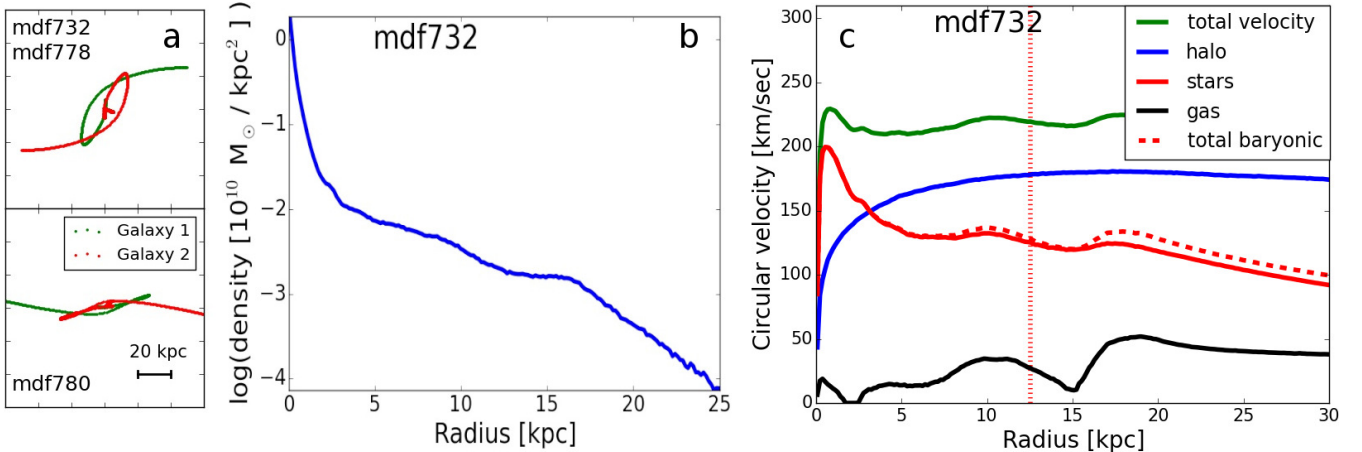


Figure 1. a: Orbits of the progenitors before the merging. b: Stellar radial surface density profile at $t=10$ Gyr. c: Circular velocity curves at $t=10$ Gyr, for the total mass, as well as separately for stars, gas, total baryonic mass and halo. The vertical red dotted line is located at 2.2 inner disk scalelengths.

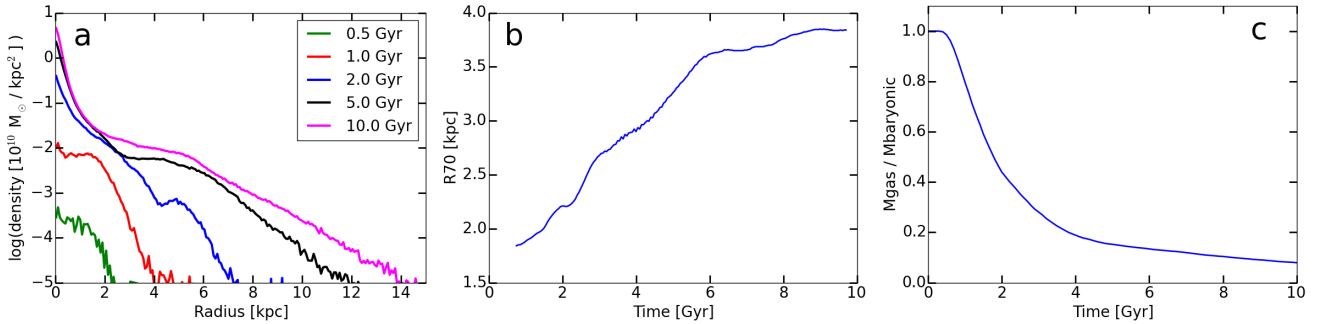


Figure 2. Properties of a simulated galaxy growing in isolation. Left: Radial surface density profile for times 0.5 (green), 1 (red), 2 (blue), 5 (black) and 10 Gyr (violet). Middle: Cylindrical radius containing 70% of the stellar mass. Right: Fraction of the gas in the disk ($|\Delta z| < 0.5$) component as a function of time.

Fig. 3 gives the morphologies at the end of the simulations². mdf778 has the largest disk extent and mdf780 the shortest. Seen face-on, all three galaxies have a clear and extended spiral structure. Let us denote by m the spiral arm multiplicity, i.e. the number of arms at any given radius. mdf778 is mainly bisymmetric ($m=2$), while mdf732 and mdf780 are $m=2$ in the inner parts and $m>2$ at larger radii, reaching $m=5$ at the edges of the disk. This increase of m with distance from the center is in good agreement with observations and was explained by Athanassoula et al. (1987, see also Athanassoula 1988 for models including accretion). These authors applied the swing amplification analytical formalism (Toomre 1981; see also reviews by Athanassoula 1984 and Dobbs & Baba 2014) to their rotation curve decompositions results and pointed out that, if the spiral structure was due to swing amplification, the arm multiplicity should increase with distance from the center. Thus the spiral structure in mdf732 and mdf780 is consistent with a swing amplification origin. Providing, however, tangible proof that these are swing amplification driven spirals is well beyond the scope of this paper.

mdf732 has an inner ring with a very asymmetric density distribution along it (Fig. 3, second row, where the lower half of the ring is clearly visible). Its semi-major axis has the same size as that of the bar and it is elongated in the same

direction, both in good agreement with inner ring observations (e.g. Buta 1995, and references therein). Good examples of such inner rings can be seen in NGC 1433 and NGC 3660. mdf778 and mdf780 have $m=2$ spirals emanating from the ends of the bar roughly perpendicular to it and then trailing behind it, again in good agreement with what happens in observed local galaxies.

The bar size in all three simulations (2.5 to 4 kpc semi-major axis) is only slightly below the average for the stellar mass in question, and well within the range of observed values for external galaxies (lowest panel of Fig. 20 in Diaz et al. 2015). It should be noted that our three models presented here have a similar stellar mass as the Milky Way, and their bar length closely matches that of the Milky Way bar. To measure the bar strength, we Fourier decomposed the projected surface density of the face-on view as in Diaz et al. and used the maximum value of the relative $m=2$ Fourier component as the bar strength (see e.g. Diaz et al. for more information on this method). For our three simulations we find values between 0.32 and 0.35, which are in good agreement with observations. However this comparison is less constraining than the one concerning the bar length, because the observed values show a very large spread (second panel of Fig. 20 in Diaz et al. 2015).

We can also make meaningful comparisons concerning the bar morphology. Combining information from three different approaches, namely simulations following bar formation in isolated disk galaxies, orbital structure theory, and observations Athanassoula (2005, see also Athanassoula 2015 for

² Figs. 3, 4 and 6 were made using the glnemo2 software (<http://projets.lam.fr/projects/glnemo2>), which, in order to display morphologies best, uses color coding corresponding to the maximum of the spatial density along the line of sight.

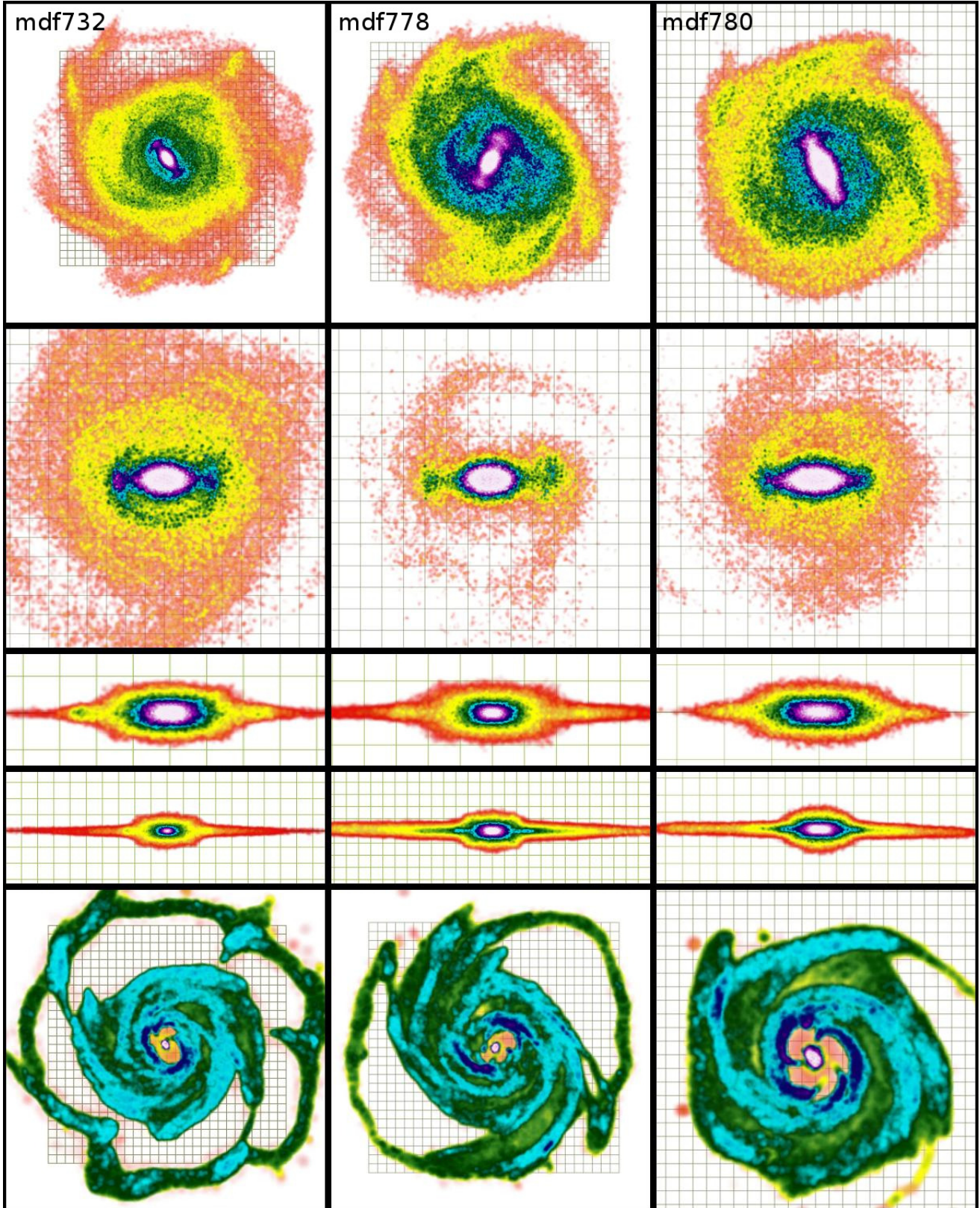


Figure 3. Morphology of the stellar (upper four rows) and gaseous (fifth row) disk components of our three fiducial simulations at $t=10$ Gyr. The uppermost panels give the face-on view and the second row zooms in the inner regions to highlight the face-on bar morphology. The fourth row shows the side-on view of the disk and the third row the side-on view of the bar region. The fifth row gives the face-on view of the gas distribution. To bring out best the features of interest (see text), we choose the color coding and linear resolution of each panel separately and include in the background a Cartesian grid with cells of 1×1 kpc size, to allow size estimates. In the second, third and fourth row the snapshot has been rotated so that the bar is along the x axis.

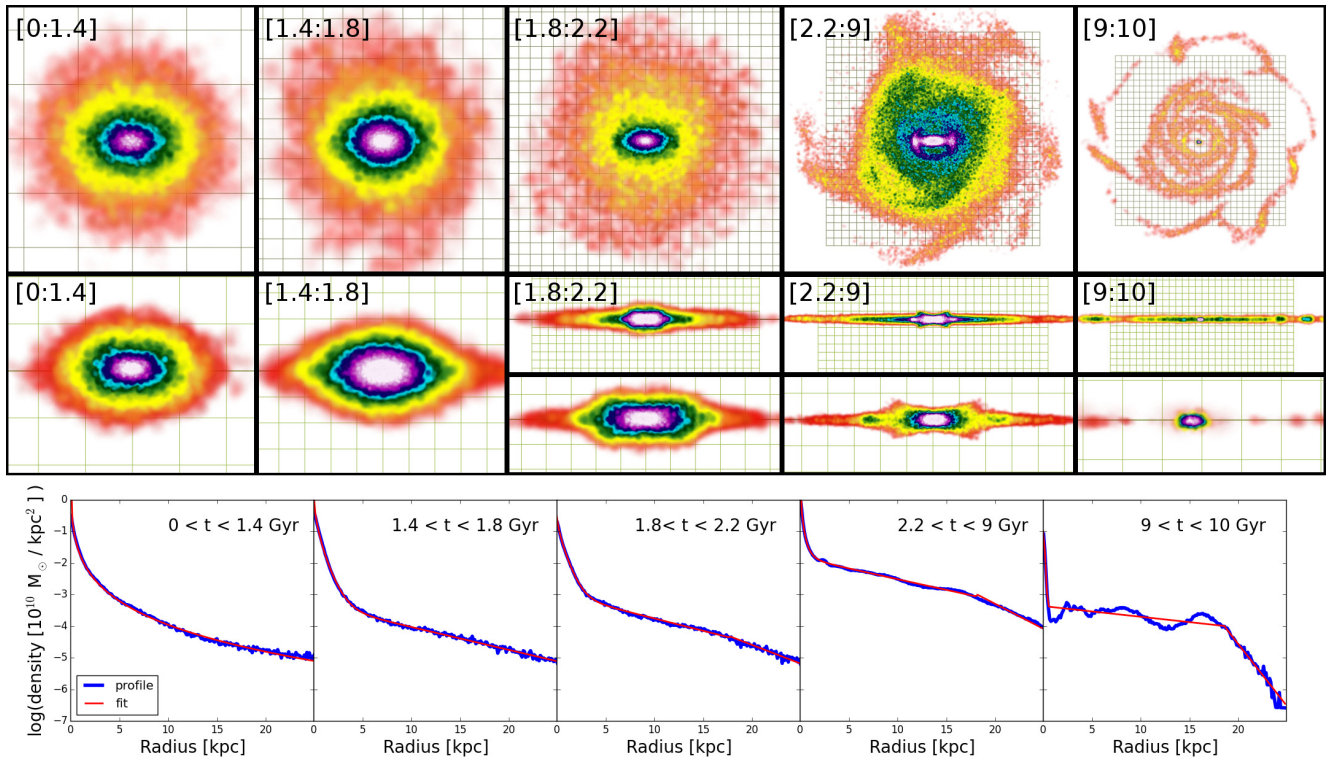


Figure 4. Five different stellar populations for mdf732 at $t=10$ Gyr, separated according to their time of birth (see text). Upper panels: Face-on views of the five populations. Middle panels: Edge-on views of the same populations. For the three youngest populations we include also a zoom of the inner parts to show best the morphology of the bar region viewed edge-on. For color coding and the background Cartesian grid see caption of Fig. 3. Lower panels: Surface density radial profiles of the five stellar populations as obtained from their face-on views (blue lines) and the corresponding decompositions (red lines). In the leftmost panel we used only one component, of Sérsic profile. The respective birth time ranges are given in the upper right corner of the lower panels.

a review, and references therein) came to the conclusion that bars have a rather complex shape. Namely their outer part is thin both when seen edge-on and face-on, while their inner part is thick again both viewed face-on and edge-on. Viewing the bars in our simulations from different angles, we find that they also have the above described morphology, arguing for a proper dynamical description of bars in our simulations and, most important, arguing that the observed bar shapes are compatible with a scenario of disk formation via major mergers.

The face-on bar morphology also agrees well with observations. In particular, the bar has ansae (Sandage 1961) and a barlens component (Laurikainen et al. 2014; Athanassoula et al. 2015). Seen side-on, the latter is usually referred to as a boxy/peanut/X bulge, but is in fact a part of the bar, i.e. consists of disk material and forms via disk instabilities (Athanassoula 2015, for a review).

The morphology of mdf778 shows a number of embedded structures, namely a bar of radial extent ~ 3 kpc, an oval of radial extent ~ 14.5 kpc outside the bar and two $m=2$ sets of spirals. The inner set is confined within the oval, while the outer one emanates from the ends of the oval, extends to larger radii (maximum ~ 16.5 kpc) and falls back to the oval thus forming an outer pseudoring. Similar embedded structures can be seen e.g. in NGC 1566. The outer pseudoring and the oval have the same low pattern speed (~ 18.5 km/sec/kpc), while the inner bar has a much higher pattern speed (~ 43 km/sec/kpc). This morphology is very similar to that of manifold-driven outer spirals and pseudorings (Romero-Gómez et al. 2006; Athanassoula et al. 2009). Furthermore, for manifold theory the pattern speed of the oval and the outer spirals should be the same, as is the case in mdf778. The ultimate test, however, can be carried out with the help of the orbits of the particles in the spirals (Athanassoula 2012). Indeed in any density wave-based theory the orbits should traverse the arms, staying longer in the arm than in the interarm. On the contrary, in manifold theory the orbits of the particles start from one of the Lagrangian points nearest to the end of the bar (L_1 or L_2) and then follow the arm shape, outlining it, until they reach the opposite side of the bar. We followed the orbits of particles in the spirals and found that they stay within the spirals and outline them, i.e. these structures are manifold spirals as in the simulations of Athanassoula (2012). There is thus conclusive evidence for manifold spirals in mdf778.

The gas has, in all three cases, a qualitatively similar morphology to the stars. Note, however, that, contrary to the stars, the gas has a minimum in the central region of the galaxy of extent comparable to, but somewhat smaller than, the bar size. Further in, at a scale of 1 kpc or less, there is a strong concentration of gas. This morphology is in good agreement both with observations and with results of previous more idealised simulations (see e.g. Fig. 2 in Athanassoula 1992).

3.4. Density and circular velocity profiles of the merger remnants

The total stellar mass at the end of the simulation is around $5 \times 10^{10} M_{\odot}$ in all three simulations, i.e. these galaxies are Milky Way-sized. Fig. 1b shows the azimuthally averaged radial projected surface density profile of mdf732 at $t=10$ Gyr. Those of mdf778 and mdf732 are qualitatively the same. The outer parts in all three cases show a downbending truncation (i.e. of Freeman type II, e.g. Freeman 1970; Erwin et al. 2005; Muñoz-Mateos et al. 2013), which is the most common amongst the truncation types: $\sim 60\%$ according to Pohlen & Trujillo (2006), or 42% according to Laine et al. (2014).

Fig. 1c shows the circular velocity curves for mdf732 at $t=10$ Gyr, both for the total mass in the galaxy, and for its basic components. It is calculated directly from the particle masses and positions in the simulation, without assuming spherical symmetry, contrary to a number of previous works. It is qualitatively the same for the other two cases. The total curve is fairly flat, with two shallow bumps due to the spirals. There is also a somewhat higher bump (15 – 20 km/sec) in the central region, due to the bulge. The ratio of the velocity due to the baryonic components to the total at 2.2 inner disk scalelengths is about 0.57 (mdf732), 0.62 (mdf778) and 0.69 (mdf780) of the total. Thus, relying on the Sackett (1997) criterion, mdf732 and mdf778 are clearly submaximal, while mdf780 is also submaximal but very near the borderline with maximum disks. Compared to the galaxies of the DISKMASS survey (Bershady et al. 2011, their Fig. 2), our three models have, for their circular velocity, amongst the highest fraction of disk mass of the survey, or even somewhat higher.

3.5. Circularity parameter

In a totally cold, perfectly axisymmetric disk, all stars will rotate with a velocity equal to the circular velocity. Stars in galactic disks, however, have some radial motion, albeit considerably less than their tangential one. At the other extreme, stars in classical bulges have strongly non-circular motions with considerable radial velocity components and with either direct or retrograde rotation. In between the two, there are stars in structures such as bars, ovals or lenses, whose motion is neither as circular as that of disk stars, nor as far from circular as that of classical bulge stars can be.

These different kinematics are reflected in the different values of the normalised angular momentum of a stellar orbit, known as the circularity parameter $\varepsilon = J_z / J_{circ}$, where J_z is the z component of the angular momentum and J_{circ} is the angular momentum of the circular orbit of the same energy (e.g. Abadi et al. 2003; Aumer & White 2013). Fig. 5a shows an example (red line) of a histogram of the number of particles as a function of their circularity for a snapshot with only a classical bulge and a disk component. This simulation is in all aspects identical to mdf732, except that no AGN feedback has been included (see Sect. 2.3 and Paper II). The classical bulge and the disk are clearly distinct and it is possible to distinguish disk from bulge stars simply by introducing a separation limit to their circularity value (ε_{lim}), which, as can be seen from Fig. 5a is situated around 0.5. We tested this kinematic way of distinguishing disk from classical bulge stars by viewing the spatial distribution of the two thus obtained populations separately and from various viewing angles and made sure that the disk is indeed adequately distinguished from the classical bulge component. After some trials, we found that $\varepsilon_{lim}=0.5$ gave quite satisfactory results and we adopted it. The stars that this method assigns to the disk(bulge) will hereafter be called ‘kinematic disk(bulge) stars’.

A related, very useful quantity is the circularity at birth (ε_{birth}). As expected, this is very near 1 for stars born in the disk, but not for stars born in the bulge. Fig. 5b shows the fraction of stars of a given birth time which are born with $\varepsilon_{birth} > \varepsilon_{lim}$, as a function of their birth time, for mdf732 and as calculated for $\varepsilon_{lim}=0.5$ (red curve). Calculations using $\varepsilon_{lim}=0.6$ and 0.7 give quasi-identical results. Note that during the merging J_{circ} can not be adequately defined, so the curve includes only times after 1.55 Gyr. This curve shows considerable structure which will be discussed in the next subsection.

3.6. Morphology and kinematics for populations of different ages

It is expected that landmark times, such as the merging time, should set clear differences between the stellar populations born before and after them and we want to check whether this is indeed the case in our simulations and what the corresponding differences are. We will assess this by examining the $t=10$ Gyr snapshot of mdf732, to which all this subsection will pertain.

An obvious choice for the first landmark time is the merging time. In major mergers, however, there is no clearly and uniquely defined merging time and it is better to define a merging period, or time range. Furthermore, we want to avoid eye estimates of such times, because they can be biased and are not reproducible. We thus define the beginning of the merging period as the earliest time after which the distance between the centers of the two merging protogalaxies is always smaller than 1 kpc (t_{bm}). Although arbitrary, this time has the advantage of being clearly defined and reproducible. We define as the center of each galaxy what is often referred to as the center of density of its halo, calculated from the positions of the halo particles with the highest local density (as defined by the distance to their nearest neighbours, e.g. Casertano & Hut 1985). We measure the distance between the two progenitor centers and find the earliest time after which this distance stays smaller than 1 kpc. For mdf732 it is around 1.4 Gyr.

As a second landmark time, hereafter t_{bd} , we chose a time associated with the beginning of the disc formation and, more specifically, the time beyond which the vast majority of stars are born with disk kinematics. We estimate this by using ε_{birth} . Fig. 5b (red line, calculated for $\varepsilon_{lim}=0.5$) shows that the fraction of kinematic disk stars increases strongly with time of birth for up to 2.2 Gyr and that about 95% of stars born after this time have disk kinematics. We thus adopt $t_{bd}=2.2$ Gyr, after verifying that this value holds also for other reasonable values of ε_{lim} . We also introduced a third time at $t_{by}=9$ Gyr, which is somewhat arbitrary and not a landmark time, but is nevertheless useful because it sets a time such that any stars born after that can be considered young and thus allows us to focus on the distribution and kinematics of the youngest stars. For our snapshot, which is at 10 Gyr, the ages of the stars born at t_{bm} , t_{bd} and t_{by} are 8.6, 7.8 and 1 Gyr, respectively.

We can thus define five time intervals: namely $[0, t_{bm}]$, $[t_{bm}, t_{hm}]$, $[t_{hm}, t_{bd}]$, $[t_{bd}, t_{by}]$ and $[t_{by}, 10]$ where $t_{hm} = 0.5(t_{bm} + t_{bd})$. We then separate the stars in five groups according to which of the above time ranges they were born in, i.e. according to their age. We thus get five separate populations, and their respective number of stellar particles is 99369, 109035, 83960, 713081 and 47376. Their face-on and edge-on views are shown in Fig. 4. Corresponding kinematic information, separately for each of these five age groups, is given in Fig. 5c, which shows the distribution of stars as a function of their circularity at 10 Gyr (ε_{10}). Examining this morphological and kinematic information together, we find a number of important results:

- Stars born before the beginning of the merging period, i.e. that are older than 8.6 Gyr, (leftmost panels of Fig. 4) are concentrated in the innermost couple of kpc and their spatial distribution and radial density profile are that of a triaxial classical bulge. They are the oldest stars in the galaxy and experienced violent relax-

ation due to the strong evolution of the potential during the merging, thus explaining their very steep radial projected density profiles (Lynden-Bell 1967). Thus major mergers provide a mechanism for classical bulge formation. Some of these stars rotate prograde and others retrograde with respect to the disk, as expected for a classical bulge (Fig. 5c). There are, however, considerably more prograde than retrograde stars, i.e. the bulge has internal rotation. This is, at least partly, due to the bar, which can make the bulge more oblate (Athanasoula & Misiriotis 2002) and give it some spin (Athanasoula 2003; Saha et al. 2012).

- Stars born during the first half of the merging period (second column of panels in Fig. 4), i.e. with ages between 8.2 and 8.6 Gyr, have a density distribution similar to that of stars born before the merging, although more extended and more flattened. The outermost isodensities of the edge-on view are cusped, as one would expect from a relatively light underlying thick disk. This is corroborated from their angular momentum distribution (green line in Fig. 5c), which shows a considerable contribution of stars with ε_{10} near but somewhat less than 1.
- Stars born during the second half of the merging period (third column of panels) have a very different density distribution from that of the two previous groups. They trace in the outer parts a disk extending well beyond the bulge region and in the inner parts a bar with a vertically thick boxy bulge (Athanasoula 2005). Their circularity distribution (Fig. 5c, red line) also shows the existence of two components, a fast rotating component, i.e. a disk; and a slower component rotating with an average ε_{10} around 0.25. Checking out the spatial distribution of the stars in the latter component we found that it is the bar (see also Sect. 3.7). Thus the stars born in this time range contribute partly to the near-axisymmetric disk and partly to the bar.
- The stars within the two last age ranges (younger than 7.8 Gyr) were born during the disk formation era and are thus part of what is commonly referred to as the disk population. This disk is extended and quite thin. Except for the axisymmetric disk, the stars in the fourth age bracket contribute also to the spirals and to the bar. For this group of stars, the ansae at the extremities of the bar are clearly visible, and at smaller radii, there is an X-like edge-on shape, as in many barred galaxies. Note that both the disk and the bar are vertically thinner than the corresponding structures in the third age bracket.

On the other hand, the stars which are younger than 1 Gyr do not participate in the bar structure, but are heavily concentrated in the spiral and ring structures, as well as in an innermost very thin structure, which can be called a disk pseudobulge (Kormendy & Kennicutt 2004; Athanasoula 2005). The latter may well exist in the third and fourth age brackets as well, but is less easily discernible in plots as in Fig. 4, because of the strong bar contribution to the central parts.

The kinematics of these two youngest age ranges (Fig. 5c) corroborate the above. In particular, they show that the stars of the fourth age range contribute partly to the disk and partly to the bar (see also Sect. 3.7). On

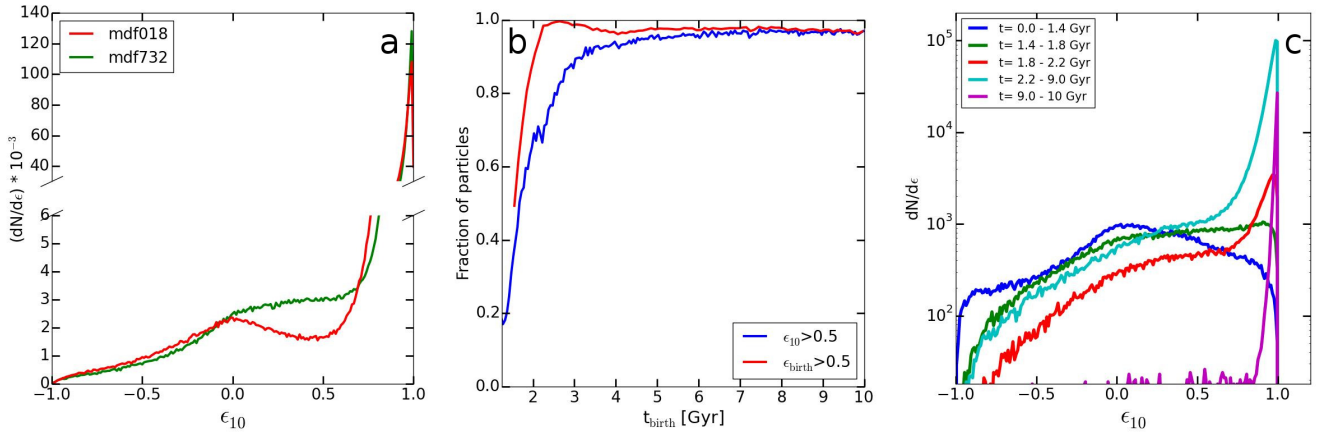


Figure 5. Identifying disk stars kinematically. Left: Distribution of the number of particles as a function of their circularity parameter for two snapshots. In one of these (red) the stars are basically either in a classical bulge, or in a disk. In the other (green) it is clear that there is a further component. Middle: fraction of stars with $\varepsilon > 0.5$ at birth (red) and at 10 Gyr (blue). Right: Distribution at $t = 10$ Gyr of particles as a function of their circularity parameter ε_{10} , given separately for the stars in each of the five time of birth brackets as in Figs. 4. The adopted bin size in both the rightmost and the leftmost panel is $\Delta\varepsilon = 0.01$.

the other hand, the stars in the youngest age bracket contribute essentially only to the disk, and more specifically (Fig. 4) to its spirals, rings and the diskly pseudobulge.

In the lower panels of Fig. 4 we show the projected density radial profiles of each of the five stellar populations, obtained from their face-on views. The oldest population is well fitted by a single Sérsic component with an index between 4.5 and 6, i.e. corresponding to a classical bulge (Kormendy & Kennicutt 2004; Drory & Fisher 2007). At the other extreme, the youngest population can be fitted by three exponential disks, the innermost one corresponding to a diskly pseudobulge, and the two next ones to the inner and outer disks, respectively. Thus, in general, the classical-bulge-to-total stellar mass ratio decreases with the age of the population from 100% to 0%.

3.7. Coupling kinematics and morphology to identify disk stars

In Sect. 3.5 we discussed a simple way of distinguishing the classical bulge population from that of the disk for snapshots with only these two components. We now extend this to snapshots with bars and/or ovals and apply it to mdf732 at $t=10$. The corresponding circularity histogram is given in Fig. 5a (green line). As expected, the distribution is now much more complex. Namely there is clearly additional material between the disk and the bulge components and applying a simple separating criterion to ε would not suffice if an important fraction of stars is in the bar component. Independent of their ε , bar stars should be considered as part of the disk component, since the bar forms from a disk instability which rearranges the disk material. We therefore conclude that not only all stars with $\varepsilon > \varepsilon_{lim}$ belong to the disk, but also a considerable fraction of those with $\varepsilon < \varepsilon_{lim}$. Thus a more elaborate analysis will be necessary for galaxies with bars.

We therefore divide stars into groups, depending on three physical properties, namely whether their time of birth is before or after t_{bd} , and on whether their kinematics at birth and at 10 Gyr are disk-like or bulge-like. The latter two are ensured by testing whether their circularity at birth and at 10 Gyr (ε_{10}) is bigger or smaller than ε_{lim} . In this section, as in Sect. 3.5, we describe results obtained with $\varepsilon_{lim} = 0.5$. We tried, however, also other values and reported some of the corresponding results in Sect. 3.8.

This division creates in total eight groups of stars, described in Table 1. Groups G1 to G4 include all stars born after t_{bd} , while groups G5 to G8 all stars born before t_{bd} . We viewed each group separately in 3D from different angles to assess its shape and morphology and we also made projected surface density profiles, both radial and vertical and for different cuts. Whenever a bar is present in the group we calculated its position angle (PA) and, comparing the PA found for all groups, we found that they all agree to within 5° , i.e. to within the accuracy of the estimates. We now consider all this information together.

Group G1 consists of stars with disk kinematics, both at birth and at 10 Gyr. Fig. 6 (leftmost panels) reveals a thin disk with a strong global spiral structure and a rather weak bar. Its projected density profile (not shown) is exponential with a small central bump due to the bar. It is thus clearly a disk population and comprises 66% of the stars.

Stars in group G2 were born with disk kinematics, and by 10 Gyr evolved to non-disk kinematics. Morphology and photometry of G2 show that 95% of G2 stars form a bar and the remaining 5% a disk component around it. The bar in G2 has roughly the same orientation and length as that of G1, but is considerably fatter horizontally. Seen edge-on, it has a clear boxy/peanut structure. Most of the stars in G2 were born very soon after t_{bd} , while those of G1, G3 and G4 are more evenly spread between t_{bd} and 10 Gyr. Thus the stars in G2 are, on average, older than the stars in other groups. Their circularity argues that they were born in the axisymmetric disk and were trapped by the bar as this grew. G2 comprises 4.56% of the stars.

G3 has disk kinematics at 10 Gyr, but not at birth, while G4 does not have disk kinematics either at 10 Gyr or at birth. The stars in those two groups are concentrated in an inner triaxial object of size roughly 1.4:0.7:0.5, whose PA is, within the errors, the same as that of G1 and G2. Thus it can be considered as an inner part of the bar, presumably part of its barlens component (Laurikainen et al. 2014; Athanassoula et al. 2015). Together, G3 and G4 comprise only 1.65% of the stars.

Groups G5 to G8 consist of stars with $t_{birth} < t_{bd}$. For most of these stars it is not possible to calculate ε_{birth} because the center of the remnant at such times is not well defined. Instead, we calculate ε at t_{bd} (ε_{bd}), because, although this is early on in the evolution, it is sufficiently late for the center of

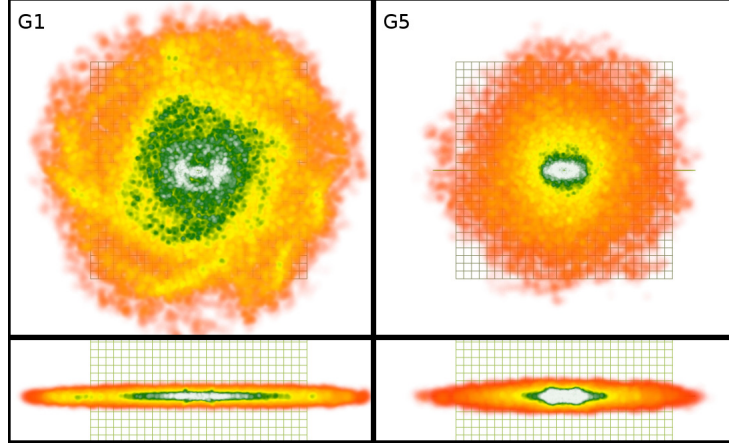


Figure 6. Components G1 and G5 at $t=10$ Gyr. Face-on (upper subpanels) and edge-on (lower subpanels) views of group G1 (left) and G5 (right) in mdf732 at 10 Gyr. All four subpanels have the same linear scale. The color coding was chosen so as to bring out best the morphological features of interest here.

Table 1
Basic properties of the eight groups

Group	Birth time	ε_{birth} , or ε_{bd}	ε_{10}	Fraction
G1	$t_{birth} > t_{bd}$	$\varepsilon_{birth} > \varepsilon_{lim}$	$\varepsilon_{10} > \varepsilon_{lim}$	0.660
G2	$t_{birth} > t_{bd}$	$\varepsilon_{birth} > \varepsilon_{lim}$	$\varepsilon_{10} < \varepsilon_{lim}$	0.046
G3	$t_{birth} > t_{bd}$	$\varepsilon_{birth} < \varepsilon_{lim}$	$\varepsilon_{10} > \varepsilon_{lim}$	0.003
G4	$t_{birth} > t_{bd}$	$\varepsilon_{birth} < \varepsilon_{lim}$	$\varepsilon_{10} < \varepsilon_{lim}$	0.013
G5	$t_{birth} < t_{bd}$	$\varepsilon_{bd} > \varepsilon_{lim}$	$\varepsilon_{10} > \varepsilon_{lim}$	0.091
G6	$t_{birth} < t_{bd}$	$\varepsilon_{bd} > \varepsilon_{lim}$	$\varepsilon_{10} < \varepsilon_{lim}$	0.040
G7	$t_{birth} < t_{bd}$	$\varepsilon_{bd} < \varepsilon_{lim}$	$\varepsilon_{10} > \varepsilon_{lim}$	0.024
G8	$t_{birth} < t_{bd}$	$\varepsilon_{bd} < \varepsilon_{lim}$	$\varepsilon_{10} < \varepsilon_{lim}$	0.123

the remnant to be clearly identified.

The stars of group G5 constitute at 10 Gyr a thick disk (Fig. 6) with no spirals and with a bar of roughly the same length and PA as that of G1, but much fatter in the plane and with no ansae. This thick disk comprises 9.08% of the stars.

Stars in group G6 basically compose a bar, similar in shape and outline to that of G5, while a few of them are in a thick disk, similar to that of G5. They comprise 3.99% of the stars.

Groups G7 has too few stars for us to be able to classify. It comprises 2.37% of the stars.

Most of the stars in group G8 belong to a flattened bulge, as argued by morphology, photometry and kinematics together. G8 isophotes have a bar like deformation in their central part, analogous to the ‘halobar’ found in the central parts of halos (Colin et al. 2006; Athanassoula 2007). G8 comprises 12.3% of the stars.

The above procedure distinguishes the disk from the classical bulge component. Groups G1, G2, G5, G6 are unambiguously linked to the disk, and this most probably is true also for G3 and G4. Indeed, they contribute mainly to the bar and, more specifically, to its inner parts. Most of group G8 is linked to the classical bulge. G7 is presumably linked to the bar, i.e. it is a disk population, but this is not as sure as for the other, above-mentioned disk components. Nevertheless, the uncertainty this entails is very small, 2 – 3%.

Note also that the stars in the thick disk are older than those in the thin one, as they were born earlier in the simulation and in a rather restricted time interval, roughly between 1.4 and 2.2 Gyr, i.e. at $t=10$ Gyr they have an age between 8.6 and 7.8 Gyr. Thus the oldest stars in this model are in the classical bulge, followed by those in the thick disk, while the youngest

are in the thin disk.

3.8. B/T mass ratio

In Table 2 we give various estimates of the B/T ratio in our three fiducial simulations at $t=10$ Gyr, as well as some close upper limits. Columns 1 and 2 give the run number and t_{bd} , respectively. Columns 3 to 8 give results for the method described in Sect. 3.7, where we extended the simple kinematic decomposition of the stars into a disk and a bulge component, to cases with a bar. There we identified most of group G8 as the classical bulge component and the corresponding B/T values are given in columns 3 to 5 of Table 2. We were, however, unable to safely identify whether G7 should be considered as a disk or a classical bulge component, so we will for safety also include an estimate based on the sum of the two components, as an upper limit (columns 6 to 8). We applied this with $\varepsilon_{lim}=0.5$ (columns 3 and 6), the value we have found to be more appropriate (Sect. 3.5) and 3.7, but also with $\varepsilon_{lim}=0.6$ (columns 4 and 7) and even $\varepsilon_{lim}=0.7$ (columns 5 and 8), the last two, and particularly the last one, being more like upper limits. As expected, the smallest values are when identifying G8 to the classical bulge and using $\varepsilon_{lim}=0.5$, while the largest are the upper limits obtained when identifying G7 and G8 together to the classical bulge component and using $\varepsilon_{lim}=0.7$. It is, however, very reassuring that the differences are small, showing that the upper limits are close to the most probable values.

Hopkins et al. (2009) introduced a different, much simpler and more straightforward method to obtain an estimate of B/T . Namely, they assume that the bulge has no global rotation and that it is the only component that includes nega-

Table 2
Classical bulge to total stellar mass ratio, calculated in four different ways.

run	t_{bd}	G8 (0.5)	G8 (0.6)	G8 (0.7)	G8 + G7 (0.5)	G8 + G7 (0.6)	G8 + G7 (0.7)	Hopkins 2009	Surface density
mdf732	2.2	0.12	0.14	0.16	0.15	0.16	0.18	0.18	0.09 – 0.15
mdf778	2.2	0.11	0.13	0.15	0.13	0.15	0.17	0.19	0.10 – 0.18
mdf780	2.8	0.18	0.21	0.24	0.22	0.24	0.27	0.25	0.09 – 0.11

tive ε values. Under these assumptions the contribution of the bulge is equal to twice the mass of particles that have negative velocities. This was introduced for disk galaxies with no bars, where the two above assumptions are very reasonable to make. However, as discussed in Sect. 3.6 and the references therein, bars, although part of the disk population, do not have disk kinematics. Furthermore, they can transmit angular momentum to the classical bulge, so that for strongly barred galaxies the estimate from this method can be considered as approximate. We apply it to our simulations and find values to within 10% of our upper limits (Table 2). It is useful to have established this agreement, because the Hopkins et al. method is easy to apply and was used in a large number of previous cases.

To get a third, independent estimate of B/T , we used a decomposition of the radial projected density profile, obtained by averaging the density in cylindrical annuli in the face-on view of the disk. This decomposition is similar to the 1D decompositions used by observers for the radial luminosity profiles and, although 1D, it is not straightforward, since the innermost regions may include either both a classical and a disky pseudobulge, or one of the two only. Depending on exactly how the decompositions are done, we find values for mdf732 between 0.09 and 0.15, for mdf778 between 0.10 and 0.18 and for mdf780 between 0.09 and 0.11, i.e. somewhat lower than, but in good agreement with the kinematic estimates.

The values of the B/T ratio we find here are considerably smaller than those found in previous simulations with no hot gas in the halo. Such simulations are well summarized in Hopkins et al. (2009), where, out of several hundred simulations, only five have $B/T \leq 0.2$, and, moreover, these five have 1:8-1:10 progenitor mass ratios. On the contrary, our B/T values are compatible with those of observed spiral galaxies and do not exclude that such galaxies were formed from major mergers. This is a big improvement over past works and is due to the existence of a hot gaseous halo in the progenitors, which is carried over in the merger remnant. Indeed, as we showed in the previous subsections, the mass of the classical bulge (B) is roughly set by the number of stars that formed before the merging. On the other hand the mass of the disk is mainly due to stars that formed after the merging. Due to the gaseous halo, the accretion of gas on the disk continues well after the merging, up to the end of the simulation and presumably well after it. It thus leads to a more extensive and more massive disk than what would be found in the absence of a gaseous halo, and, therefore, smaller B/T values. Comparisons for more simulations and the effect of various progenitor properties and orbital parameters on the B/T values will be given elsewhere.

Observations show that there are spirals, in particular relatively small late types, with no, or hardly any, classical bulge (Kormendy et al. 2010). Our own Galaxy has a classical bulge of low mass (e.g. Shen et al. 2010; Ness et al. 2013a,b), but it

is premature to state that it has no classical bulge at all. Our simulations produced considerably lower B/T values than previous ones considering major mergers. So far, however, none of our simulations gave results compatible with a total lack of classical bulge. This is a general problem of all disk galaxy formation studies and may be solved by changing the feedback recipes, as attempted in cosmological simulations (e.g. Brook et al. 2012; Brooks & Christensen 2015). Here let us simply note that major mergers should be rarer in low density environments, thus if bulgeless disks are found solely, or predominantly, in such environments their hosts may well not be major merger remnants. Moreover, our aim here is to test whether major mergers may produce disk galaxies, but certainly not to show that they are the only way of making them. Thus it is not necessary for our scenario to be able to form disk galaxies with no classical bulge at all. .

3.9. The thick disk component

When examining the group G5 in mdf732 at 10 Gyr (Sect. 3.7), we found that its stars form a thick disk (Fig. 6). We will now discuss its properties further and compare them to those of observed thick disks. Such a comparison can only be approximate because other groups may also host some thick disk stars. For example, thick disk formation will not stop abruptly at time t_{bd} , but will continue at subsequent times, albeit presumably at a tapered rate. Moreover, some stars born in the thin disk will be vertically heated, e.g. by the spirals, and thus contribute to the thick disk. Yet it makes sense to use G5 for comparisons with observations, because it is defined using physical criteria (Sect. 3.7) and, furthermore, it is a main, presumably *the* main, contributor to the thick disk. We will thus use here group G5 as a proxy, and loosely refer to it as the thick disk component. Note also that even in observations there is more than one way to define the thick disk. Thus Yoachim & Dalcanton (2006), Comerón et al. (2011b, 2012) and Streich et al. (2015) use different methods and/or different fitting functions, thus introducing considerable differences in the results.

In the disk formation scenario which we consider, the thick disk forms naturally, in agreement with the observational claim of thick disk (near-)ubiquity (Yoachim & Dalcanton 2006; Comerón et al. 2011a, but see also Streich et al. 2015).

Contrary to the thin disk, the simulated thick disk has no spirals, or then of such low amplitude that they are not discernible by eye. This should be linked to the fact that both density wave (Lin 1967) and swing amplification theories (Toomre 1981) show that hotter and thicker disks will harbour lower amplitude spirals. A similar result presumably holds also for a manifold origin, because it is more difficult to confine a hot stellar population than a cold one (see also Romero-Gómez et al. 2006), but no specific quantitative study has yet been made.

By definition, the stars in group G1 were born after t_{bd} , while those in group G5 before that. Thus the stars in the thick disk are older than the stars in the thin disk, in agreement with

observations (e.g. Mould 2005; Yoachim & Dalcanton 2008; Comerón et al. 2015).

The bar in the thick disk has the same length and orientation as that of the thin one, but is much thicker in the disk plane than that of G1, as would be expected from previous work (Athanasoula 1983, see also Athanasoula 2003), where it was shown that the bar is thicker in the disk plane in the case of hotter disks. Note also that the bar in the thick disk has no ansae and, viewed side-on, it has a boxy/peanut bulge with a considerably larger vertical extent than that of the thin bar. According to this scenario, and since the thin and the thick disks co-exist, the bar component in observed galaxies will include contributions from both thin and thick disks, so that various parts of the bar may have different mean stellar ages.

Observations (Yoachim & Dalcanton 2006; Comerón et al. 2012) show that the ratio of thick to thin disk mass is a decreasing function of the circular velocity, so that more massive galaxies have a relatively less massive thick disk. Yoachim & Dalcanton (2006, see caption of their Fig. 22) provide a simple fitting formula for this decrease, which, although poorly constrained for massive galaxies, has the advantage of fitting the whole mass range. Applying it for $V_{\text{circ}}=210$ km/sec, we find a ratio of thick to thin disk masses of 0.10, which, given the uncertainties due to the extrapolation, is in good agreement to the value of 0.14 we found in Sect. 3.7.

We calculated the mean tangential velocities of G1 and G5 in an annulus between 5 and 15 kpc from the center. This adopted radial range is not optimum, since it includes mainly large radii where the difference of the two means will be relatively small, but it was chosen so as to avoid the bar region, where the kinematics depend mainly on the strength of the bar, and only indirectly on the disk thickness. We find 209 and 197 km/sec for the thin and the thick disk respectively, values which are as expected in both sense and amplitude. They are also in agreement with the results of Yoachim & Dalcanton (2008), who find that for the higher mass galaxies in their sample, they fail to detect differences between the thin and the thick disk kinematics.

3.10. On the role of the halo gas

As already discussed in Sect. 2 and 3.1, our protogalaxies acquire a baryonic (stellar plus gaseous) disk before the merging. Thus our simulations describe the merging of two disk protogalaxies with a halo composed of DM and gas. We will here examine the role of the halo gas on the formation and evolution on the ensuing disk galaxy by tracking the origin of gaseous and stellar particles and by comparing cases with and without halo gas. We will thus use two different approaches:

3.10.1. Tracking the origin of gaseous and stellar particles in the disk

In this first approach we will use mdf732 to disentangle the gas which would be present in simulations with a gaseous disk but no gas in the halo, from the gas which is present in simulations including a gaseous halo (i.e. all the gas in our simulations). We track each of these two separately and follow how each one evolved up to 10 Gyr, i.e. the end of the run. We also take into account that each gas particle may have stayed in gaseous form or it may have turned into a stellar particle.

In order to disentangle the gas origin we use a snapshot at $t=0.85$ Gyr. This roughly corresponds to the time of the apocenter following the first pericenter. We also tried other times, between 0.7 and 0.9 Gyr and found qualitatively the same and quantitatively very similar results. Since the equatorial planes

of the two protogalaxies coincide with the orbital plane, we can roughly define as halo gas all gas particles with $|\Delta z| > 1$ kpc, so that the gas which would be present in a simulation with no gaseous halo is only the gas with $|\Delta z| < 1$ kpc. The latter includes the gas in the two protogalactic disks before the merging as well as the gas in the tails formed during the interaction. It is important to include the gas in the tails because it moves initially outwards but eventually turns back at larger distances from the center and falls back towards the remnant disk. We can thus roughly assume that by tracking the gas with $|\Delta z| < 1$ kpc we follow the gas that would be present in a simulation with no gas in the halo. Of course the slab $|\Delta z| < 1$ kpc will also contain some halo gas, so that the above rough decomposition gives an upper limit of what the gas in cases with no halo gas can do. This upper limit, however, should be quite near the actual value.

Fig. 7a shows the mass found in the remnant disk still in gaseous form as a function of time, both including (red line) and excluding (blue line) the gas in the halo. The former shows a much weaker decrease with time (less than a factor of 2.5 between 3 and 10 Gyr) than the latter (more than a factor of 10 in the same time). This is clearly due to the gas accreted from the halo, which leads to much more gas-rich disks all through the simulation and a slower gas mass decrease.

Fig. 7b gives a similar comparison, but now for the stars. Here we compare the stellar mass formed in cases with no gaseous halo (blue line) to all disk stars (independent of the origin of the gas they were born from – red line). The latter shows a steady increase with time, compared to the former which is nearly constant. More specifically we witness an increase by a factor of 2.4 for the latter compared to barely a factor of 1.1 for the former.

Fig. 7c gives the ratio of gaseous to total baryonic mass as a function of time. This decreases from 0.37 at 3 Gyr to 0.092 at 10 Gyr when halo gas accretion is included, while it decreases from 0.1 to 0.01 in the same time range when accretion from the halo is not included.

To summarise, both the stellar and the gaseous disk are more massive when the accretion from the halo gas is taken into account, as expected, while the gas fraction in the disk is more compatible with that of spiral galaxies.

3.10.2. A test simulation

To deepen our understanding of the effect of the halo gas component on the disk galaxy formation and evolution we ran a further simulation. As initial conditions we used a snapshot of simulation mdf780 at $t=1.77$ Gyr, in which we replaced the low density gas particles (local density $< 5 \times 10^{-4} M_{\odot}/\text{pc}^3$) by collisionless particles. These had the same mass and positions as the gas particles they replaced, and their velocity was taken from the velocity distribution of the halo (as e.g. in Rodionov et al. 2009), in order to preserve as much as possible the dynamical equilibrium of the system. We also verified that this gas was essentially in the halo and that the gas in the disk and in the tidal tails was not affected by this change. This is run mdf223, which we compare to mdf780 in Fig. 8. Even a cursory glance shows that there is quite important differences between their mass distributions. The disk in mdf780 is much more extended and massive than that of mdf213. These results are in agreement with what we already discussed from the analysis of mdf732 in Sect. 3.10.1 and the two together show that the gaseous halo plays a crucial role in the formation and evolution of the disk.

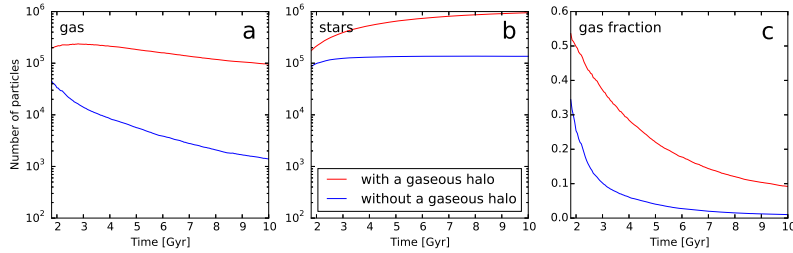


Figure 7. Number of gaseous (left panel) and stellar (middle) particles in the disk component as a function of time. The rightmost panel shows the gas fraction, again as a function of time. Red (blue) stand for a merging of two progenitors with (without) a gaseous halo (see Sect. 3.10.1 for a description).

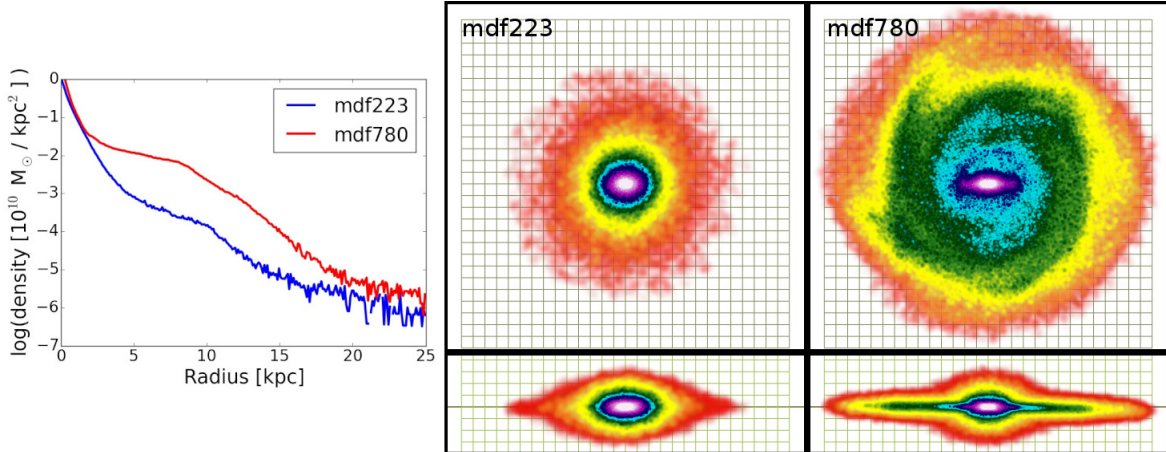


Figure 8. Comparison of two simulations, one with (mdf780) and the other without (mdf223) a hot gaseous halo, both at time $t=10$ Gyr. Left: The radial projected stellar surface density profiles. Middle: Face-on (upper) and edge-on (lower subpanels) views for mdf223. Right: Same for mdf780. Note the big difference in the disk extent and in its mass relative to the classical bulge component.

4. A SIMPLE SCENARIO FOR THE FORMATION OF DISK GALAXIES

Putting together the results from the previous section, we can outline the following simple scenario of disk formation via major mergers.

Two spherical protogalaxies, composed of DM and hot gas, are on an orbit leading to a merger. From the onset of the simulation, however, the gas in each halo cools radiatively and, getting out of equilibrium, falls inwards. Its density increases locally and the first stars form. Thus, the progenitors gradually acquire a disk and by the time the merging starts, the two progenitors can be described as disk protogalaxies, i.e. disk galaxies which are smaller and more gas rich than present day galaxies.

During the merging period the potential changes drastically during a relatively short period of time. Therefore most of the stars which were formed before the beginning of the merging period will undergo violent relaxation and will form a spheroidal bulge. Concurrently, a considerable fraction of the gas in the progenitor falls inwards and forms stars in the same bulge area. Most of the remaining disk gas moves outwards and forms, together with some of the outermost stars, extended tails.

A number of stars, particularly those born near the end of the merging period, will not be part of the bulge, but will form a thick disk.

After the end of this merging phase, the evolution stops being violent and becomes secular. The material in the tails gradually reach apocenter and fall back towards the center of the remnant. However, most of the gas accreting on the disk comes from the hot gaseous halo and forms a thin extended

disk. In our three fiducial simulations this disk is bar unstable and a bar component grows concurrently with the disk. As in isolated disk simulations (Athanasoula 2015, for a review), this bar is composed of two parts an outer thin bar and an inner thick one. The latter is often referred to as the boxy/peanut/bulge but in fact is only the inner part of the bar grown from disk instabilities. The stars forming during the most recent times can be found in spirals, mainly grand design, as well as in a diskly pseudobulge.

Very schematically, the formation of disk galaxies from a major merger can be seen as a three-stage process. The stars born before, or at the beginning of the merging period will undergo very strong and abrupt changes of the potential in which they evolve and therefore be subject to violent relaxation. They will constitute the classical bulge, and will be the oldest in the galaxy. Stars born around the end of the merging period will still feel considerable changes of the potential. These, however, are less strong and abrupt than those felt by the older stars, so that they are only strongly shuffled and end up in a thick disk component. Stars which are born well after the end of the merging period are born in near-circular orbits near the equatorial plane of the galaxy and form the thin disk. Thus, according to our scenario, the sequence from classical bulge, to thick disk, to thin disk should be a sequence of stellar age, with the stars in the classical bulge being the oldest and those in the thin disk being the youngest. The amount of perturbation they went through also decreases along the same sequence, from violent relaxation, to simple secular evolution. Furthermore their vertical thickness also decreases in the same way, from the triaxial classical bulge spheroid, to a thick and then a thin disk.

Of course once the thin disk is even partially in place, its evolution will be driven by its instabilities which will form the observed components of disk galaxies, such as bars, spirals, lenses, rings etc. Gas will be pushed inwards, either by the bar or spirals, or by various asymmetries in the merging or post-merging phases. This can form the disk pseudobulge, which will, therefore, have a considerable amount of young stars and gas, but also include some older stars.

Thus the major merger scenario can account for many observational constraints.

5. SUMMARY AND CONCLUSIONS

This paper is the first of a series using N-body simulations to test whether the remnants of early major mergers can be spiral galaxies. Our main improvement with respect to previous work on this specific subject is that each of the progenitor galaxies in our simulations has a hot gaseous halo component and these merge together in a hot gaseous halo of the merger remnant. We also have a larger number of particles, by as much as an order of magnitude compared to many previous simulations. Furthermore, we introduced a simple but effective AGN feedback model, which quenching star formation avoids excessive central mass concentrations of the remnants, thus leading to realistic shapes of the inner part of their rotation curves and allowing bars to form.

Contrary to previous work on this specific subject, our initial conditions do not mimic local galaxies, they are spherical distributions of DM and gas. Before including them in the merging simulations, we followed their growth in isolation and found that during the first few Gyr they form disk protogalaxies compatible with observations of disk galaxies at intermediate redshifts. In particular, they are dynamically less relaxed and much smaller than local galaxies, growing inside-out at a rate which is strong initially but decreases with time. They are also much more gas rich than local galaxies, with a gas fraction which decreases steadily with time, again at a faster rate during the earlier times. Thus what merges in our simulations are disk protogalaxies, more compatible with observations of galaxies at intermediate redshifts than with local ones.

To get both qualitative and quantitative estimates of the effect of the gaseous halo on the disk formation process in our scenario we used two different approaches. Both showed clearly that the presence of the gaseous halo leads to stellar and gaseous disks which are more massive and more extended. Star formation continues all through the simulation, so that there will be young stars at all times, as expected. On the contrary, if no gaseous halo is included, the amount of gas decreases with time and star formation grinds to a halt. Thus our improvement will allow us to discuss elsewhere in this series the chemical evolution and population synthesis in galactic disks.

In our model, the progenitor disks are destroyed by violent relaxation during the merging, but a new disk forms in the remnant, mainly composed of material that is gradually accreted from the halo after the merging and up to the present time. Thus, the formation of the bulge is due to a violent event, the merging, while the formation of the disk is secular. Furthermore, the existence of a sizeable disk in the major merger remnant by the end of the simulation does not argue that the disks survived major mergers, but that a new disk forms after the merging. This will have implications for the chemical composition and colors of the galactic disk, as expected, and as we will discuss in a future paper.

All three of our remnant examples have a thin, extended disk and a classical bulge. The projected radial density profiles of the disks are of type II, i.e. have downbending truncations. The rotation curves are flat and show that the disk is submaximum in all three cases, albeit only borderline so in one of the three. The disk has substructures, which our resolution allows us to examine. In particular we find bars, spirals, ovals, rings and disk pseudobulges. In all cases, their morphology is very realistic. Bars have both a thin and a thick component, the latter being better known as a boxy/peanut bulge. They also have ansae. Note that all three types of bulges – classical, disk pseudobulges and boxy/peanut/X – are simultaneously present, as in observations (e.g. Erwin 2008, and references therein), as could be expected from the scenario we present here. We also found ovals and realistic inner and outer rings and pseudorings. By following the orbits of individual stellar particles in the simulations, we found conclusive evidence that at least in one of the three simulations the spiral is of manifold origin.

A separate thick disk component forms naturally in our simulations, as would be expected from the very common, if not ubiquitous appearance of these structures in observed disk galaxies. Their properties – such as their mass, mean tangential velocities, substructures and the age of their stellar populations – are compatible with both observations and previous theoretical work.

We introduced a new method for distinguishing the bulge stellar particles from those of the disk and its substructures. This couples information from stellar ages, kinematics, morphology, spatial distribution and projected surface density profiles. It is rather precise, albeit not straightforward. We compare the results with those of a straightforward method proposed by Hopkins et al. (2009) and find very good agreement for cases with no bar. This agreement, however, becomes less good for cases with bars and can be unsatisfactory for cases with very strong bars.

In our three fiducial simulations, we find that at $t=10$ Gyr, the mass of the classical bulge is, on average, between 10 and 20% of the total stellar mass, i.e. values much smaller than in previous works, as required in order to agree with the lower B/T values of spiral galaxies. This improvement is a corollary of the existence of a hot gaseous halo in our initial conditions, as this entails a slow formation and evolution of a massive disk. Indeed the mass of the classical bulge is set by the number of stars formed before the merging, i.e. depends relatively little on the existence of the gaseous halo, while the thin disk is much more massive in cases with such a component.

This, however, does not mean that all disk galaxies which are remnants of major mergers of protogalaxies with a gaseous halo will have such small classical bulges. We will present many examples with more massive classical bulges elsewhere. Note also that we were unable to form disk galaxies with no classical bulge at all. This is in agreement with the discussion in Kormendy et al. (2010), which argues that such bulgeless galaxies would be mainly found in low density environments where major mergers would be rather rare.

We are also able to build a sequence of components, according to the time of formation of their stars. The oldest stars are found in the classical bulge, since they are actually formed before the merging. The stars in the thick disk are the next to form, followed by the intermediate age stars in the disk and bar. The youngest stars can be found in the spirals and in a disk pseudobulge. Furthermore, based on the ensemble of our results, we are able to propose a simple scenario for the

formation of disk galaxies in major mergers.

We made a number of comparisons of our results with observations of spiral galaxies and found nothing that could exclude the possibility of forming such galaxies in major mergers of disk galaxies. We can thus consider the work presented here as a first “proof of concept” that remnants of major mergers of two disk galaxies with a hot gaseous halo component can be spiral galaxies. Elsewhere we will discuss more examples with various morphologies, B/T ratios, and kinematics, as well as specific dynamical aspects. We will thus be able to make more complete and detailed comparisons with observations which, in turn, will allow us to answer fully whether major mergers are a possible way of making disk galaxies, or not.

APPENDIX

In this appendix we briefly review the nomenclature we use in this paper regarding bulges. More extended discussion on this and specific references can be found in Kormendy & Kennicutt (2004), Athanassoula (2005,2015), Drory & Fisher (2007), and Fisher & Drory (2015).

Bulges are not a homogeneous class of objects. We here distinguish between classical bulges and disky pseudobulges. The former have a spheroidal shape and a Sérsic projected density profile with a large exponent, above say 2.5. They rotate relatively little, with V_{max}/σ values that are consistent with isotropic oblate rotators. On the other hand, disky pseudobulges have the shape of a thin disk and a Sérsic profile exponent below 2.5. They show rotation and also they harbour structures like inner bars and inner spirals. When we discuss here the B/T ratio, we refer to the ratio of the classical bulge mass to the total stellar mass.

Boxy/peanut/X bulges are called Boxy/peanut/X because of their shape and are called bulges because they protrude out of the galactic equatorial plane. Physically, however, they are just the thick part of the bar. The same structure, seen face-on, is often called a barlens. Although they are clearly not classical bulges, boxy/peanut/X bulges should *not* be referred to as pseudobulges, so as not to be confused with disky pseudobulges.

ACKNOWLEDGMENTS

We thank Albert Bosma and F. Hammer for stimulating discussions, and Volker Springel for the version of GADGET used here. We also thank an anonymous referee for their useful report which helped us improve the presentation of this paper. We acknowledge financial support from CNES (Centre National d’Etudes Spatiales, France) and from the EU Programme FP7/2007-2013/, under REA grant PITN-GA-2011-289313, as well as HPC resources from GENCI/TGCC/CINES (Grants x2013047098 and x2014047098) and from Mesocentre of Aix-Marseille-Université (program DIFOMER).

REFERENCES

- Abadi, M., Navarro, J., Steinmetz, M., Eke, V. 2003, ApJ, 597, 21
 Athanassoula, E. 1983, in Internal kinematics and dynamics of galaxies, ed. E. Athanassoula, Dordrecht, D. Reidel Publishing Co., 243
 Athanassoula, E. 1984, PhR, 114, 319
 Athanassoula, E. 1988, in Towards understanding galaxies at large redshift, Dordrecht, Kluwer Academic Pub., 1988, 111
 Athanassoula, E. 1992, MNRAS, 259, 345
 Athanassoula, E. 2003, MNRAS, 341, 1179
 Athanassoula, E. 2005, MNRAS, 358, 1477
 Athanassoula, E. 2007, MNRAS, 377, 1569
 Athanassoula, E. 2012, MNRAS, 426, 46
 Athanassoula, E. 2013, in Secular Evolution of Galaxies, ed. J. Falcón-Barroso & J. H. Knapen, Cambridge, UK: Cambridge University Press, 305
 Athanassoula, E. 2015, in Galactic Bulges, ed. E. Laurikainen, R. Peletier and D. Gadotti, Springer Verlag, Germany, p. 391
 Athanassoula, E., Bosma, A., Papaioannou, S. 1987, A&A, 179, 23
 Athanassoula, E., Laurikainen, Salo, H., Bosma, A. 2015, MNRAS, 454, 3843
 Athanassoula, E., Misiriotis, A. 2002, MNRAS, 330, 35
 Athanassoula, E., Romero-Gómez, M., Masdemont, J. J. 2009, MNRAS, 394, 67
 Aumer, M., White, S. 2013, MNRAS, 428, 1055
 Barnes, J. 1998, in Galaxies: Interactions and Induced Star Formation, ed. D. Friedli, L. Martinet and D. Pfenniger, Springer-Verlag Berlin/Heidelberg, p. 275
 Barnes, J. 2002, MNRAS, 333, 481
 Bershady, M., Martinsson, T., Verheijen, M., et al. 2011, ApJL, 739, 47
 Bondi, H. 1952, MNRAS, 112, 195
 Bondi, H., Hoyle, F. 1944, MNRAS, 112, 195
 Borlaff, A., Eliche-Moral, M. C., Rodríguez-Pérez, C., et al. 2014, A&A, 570, 103
 Bouwens, R., Illingworth, G., Blakeslee, J. 2004, ApJ, 611, L1
 Brook, C., Stinson, G., Gibson, et al., 2012 MNRAS, 419, 771
 Brooks, A., Christensen, C. 2015, in Galactic Bulges, ed. E. Laurikainen, R. Peletier and D. Gadotti, Springer Verlag, Germany, 317
 Buta, R. 1995, ApJS, 96, 39
 Buta, R., Sheth, K., Athanassoula, E., et al. 2015, ApJS, 217, 32
 Casertano, S., Hut, P. 1985, ApJ, 298, 80
 Colin, P., Valenzuela, O., Klypin, A. 2006, ApJ, 644, 687
 Comerón, S., Elmegreen, B. G., Knapen, J. H., et al. 2011b, ApJ, 741, 28
 Comerón, S., Elmegreen, B. G., Salo, H., et al. 2012, ApJ, 759, 98
 Comerón, S., Knapen, J. H., Sheth, K., et al. 2011a, ApJ, 729, 18
 Comerón, S., Salo, H., Janz, J., Laurikainen, E., Yoachim, P. 2015, A&A, 584, 34
 Conselice C., Mortlock A., Bluck A. F., Grützbauch R., Duncan, K. 2013, MNRAS, 430, 1051
 Cox, T. J., Jonsson, P., Primack, J. R., Somerville, R. S. 2006, MNRAS, 373, 1013
 Cuddeford, P. 1991, MNRAS, 253, 414
 Cullen, L., Dehnen, W. 2010, MNRAS, 408, 669
 Daddi, E., Bournaud, F., Walter, F., et al. 2010, ApJ, 713, 686
 Dahlen, T., Mobasher, B., Dickinson, M. et al. 2007, ApJ, 654, 172
 Díaz-García, S., Salo, H., Laurikainen, E., Herrera-Endoqui, M. 2015, arXiv:1509.06743
 Dobbs, C., Baba, J. 2014, PASA, 31, id.e035
 Drory, N., Fisher, D. B. 2007, ApJ, 664, 640
 Elmegreen, B. G., Elmegreen, D. M., Vollbach, D. R., Foster, E. R., Ferguson, T. E. 2005, ApJ, 634, 101
 Erb D. K., Steidel C. C., Shapley A. E., et al. 2006, ApJ, 646, 107
 Erwin, P. 2008, in Formation and Evolution of Galaxy Bulges, ed. M. Bureau, E. Athanassoula, B. Barbuy, IAU Symp., 245, 113
 Erwin, P., Beckman, J. E., Pohlen, M. 2005, ApJ, 626, L81
 Eskridge, P. B., Frogel, J. A., Pogge, R. W., et al. 2000, AJ, 119, 536
 Ferrarese L., Merritt D. 2000, ApJ, 539, L9
 Ferguson, H., Dickinson, M., Giavalisco, M. 2004, ApJ, 600, L107
 Fisher, D., Drory, N. 2015, in Galactic Bulges, ed. E. Laurikainen, R. Peletier and D. Gadotti, Springer Verlag, Germany, 41
 Freeman, K. C. 1970, ApJ, 160, 811
 Gebhardt K., Bender, R., Bower, G., et al. 2000, ApJ, 539, L13
 Genzel, R. A., Tacconi, L. J., Lutz, D., et al. 2015, ApJ, 800, 20
 Governato, F., Brook, C. B., Brooks, A. M., et al. 2009, MNRAS, 398, 312
 Hammer, F., Flores, H., Zheng, X. Z., Liang, Y. C., Cesarsky, C. 2005, A&A, 430, 115
 Hammer, F., Flores, H., Puech, M., et al. 2009a, A&A, 507, 1313
 Hammer, F., Flores, H., Yang, Y. B., et al. 2009b, A&A, 496, 381
 Hayward, C., Torrey, P., Springel, V., Hernquist, L., Vogelsberger, M. 2014, MNRAS, 442, 1992
 Hopkins, P. F. 2013, MNRAS, 428, 2840
 Hopkins, P. F. 2014, Astrophysics Source Code Library, record ascl:1410.003
 Hopkins, P. F. 2015, MNRAS, 450, 53
 Hopkins, P. F., Cox, T. J., Younger, J. D., Hernquist, L. 2009, ApJ, 691, 1168

- Hopkins, P. F., Cox, T. J., Hernquist, L., et al. 2013, *MNRAS*, 430, 1901
- Hopkins, P. F., Quataert, E. 2010, *MNRAS*, 407, 1529
- Hoyle, F., Lyttleton, R. A. 1939, *PCPS*, 35, 405
- Kannan, R., Macciò, A. V., Fontanot, F., et al. 2015, *MNRAS*, 452, 4347
- Kormendy, J. 2013, in *Secular Evolution of Galaxies*, ed. Jesús Falcón-Barroso & Johan H. Knapen, Cambridge, UK: Cambridge University Press, 2013, 1
- Kormendy, J., Drory, N., Bender, R., Cornell, M. 2010, *ApJ*, 723, 54
- Kormendy, J., Kennicutt R. C., Jr. 2004, *ARA&A*, 42, 603
- Knapen, J. H., Shlosman, I., Peletier, R. F. 2000, *ApJ*, 529, 93
- Laine, J., Laurikainen, E., Salo, H., et al. 2014, *MNRAS*, 441, 1992
- Laurikainen, E., Salo, H., Athanassoula, E., Bosma, A., Herrera Endoqui, M. 2014, *MNRAS*, 444, L80
- Lin, C. C. 1967, *Annual Review of Astronomy and Astrophysics*, 5, 453
- Leroy A. K., Walter F., Brinks E., et al. 2008, *AJ*, 136, 2782
- Lotz, J., Jonsson, P., Cox, T., Primack, J. 2010, *MNRAS*, 404, 590
- Lynden-Bell, D. 1967, *MNRAS*, 136, 101
- McMillan, P., Dehnen, W. 2007, *MNRAS*, 378, 541
- Menéndez-Delmestre, K., Sheth, K., Schinnerer, E., Jarrett, T., Scoville, N. 2007, *ApJ*, 657, 790
- Miller, M., Bregman, J. 2015, *ApJ*, 800, 14
- Mooster, B. P., Macciò, A. V., Somerville, R. S., Naab, T., Cox, T. J. 2011, *MNRAS*, 415, 3750
- Mould, J. 2005, *ApJ*, 129, 698
- Muñoz-Mateos, J. C., Sheth, K., Gil de Paz, A., et al. 2013, *ApJ*, 771, 59
- Ness, M., Freeman, K., Athanassoula, E., et al. 2013a, *MNRAS*, 430, 836
- Ness, M., Freeman, K., Athanassoula, E., et al. 2013b, *MNRAS*, 432, 2092
- Pohlen, M., Trujillo, I. 2006, *A&A*, 454, 759
- Querejeta, M., Eliche-Moral, M. C., Tapia, T., et al. 2015, *A&A*, 573, A78
- Robertson, B., Bullock, J. S., Cox, T. J., et al. 2006, *ApJ*, 645, 986
- Rodionov, S., Athanassoula, E., Sotnikova, N. 2009, *MNRAS*, 392, 904
- Rodríguez, M., Puech, M., Hammer, F., Rothberg, B., Flores, H. 2012, *MNRAS*, 421, 2888
- Romero-Gómez, M., Masdemont, J. J., Athanassoula, E., García-Gómez, C. 2006, *A&A*, 453, 39
- Sackett, P. 1997, *ApJ*, 483, 103
- Sandage, A. 1961, *The Hubble Atlas of Galaxies* (Washington: Carnegie Institution)
- Saha, K., Martínez-Valpuesta, I., Gerhard, O. 2012, *MNRAS*, 421, 333
- Schweizer, F. 1998, in *Galaxies: Interactions and Induced Star Formation*, ed. D. Friedli, L. Martinet and D. Pfenniger, Springer-Verlag Berlin/Heidelberg, p. 105
- Scoville, N., Sargent, A., Sanders, D., Soifer, B. 1991, *ApJ*, 366, 5
- Shen, J., Rich, M., Kormendy, J., et al. 2010, *ApJ*, 720, 72
- Silk, J., Mamon, G. 2012, *RAA*, 12, 917
- Springel, V. 2005, *MNRAS*, 364, 1105
- Springel, V., Hernquist, L. 2002, *MNRAS*, 333, 649
- Springel, V., Hernquist, L. 2003, *MNRAS*, 339, 289
- Springel, V., Hernquist, L. 2005, *ApJ*, 622, 9
- Springel, V., Di Matteo, T., Hernquist, L. 2005, *MNRAS*, 361, 776
- Streich, D., de Jong, R., Bailin, J., et al. 2016, *A&A* 585, A97
- Tacconi L., Genzel, R., Neri, R., et al. 2010, *Natur*, 463, 781
- Thacker, R., MacMackin, C., Wurster, J., Hobbs, A. 2014, *MNRAS*, 443, 1125
- Toomre, A. 1981, in *The structure and evolution of normal galaxies*, Fall, S. M. and Lynden-Bell, D., ed., Cambridge and New York, Cambridge University Press, 111
- Toomre, A., Toomre, J. 1972, *ApJ*, 178, 623
- Torrey, P., Vogelsberger, M., Sijacki, D., Springel, V., Hernquist, L. 2012, *MNRAS*, 427, 2224
- Wang, J., Hammer, F., Athanassoula, E. et al. 2012, *A&A*, 538, 121
- Yoachim, P., Dalcanton, J. 2006, *AJ*, 131, 226
- Yoachim, P., Dalcanton, J. 2008, *ApJ*, 682, 1004